Supplemental Figures and Tables

Lipid metabolic reprogramming extends beyond histological tumor demarcations in human operable pancreatic cancer

Juho Pirhonen[1,2,*], Ábel Szkalisity[1,2,*], Jaana Hagström[3,4], Yonghyo Kim[5,6,7,8], Ede Migh[9], Mária Kovács[9], Maarit Hölttä[1,2], Johan Peränen[1,10], Hanna Seppänen[8,11,12], Caj Haglund[11,12], Jeovanis Valdés[5,6,8], Melinda Rezeli[5,6], Johan Malm[13], Peter Horvath[9,14,15], György Markó-Varga[5], Pauli Puolakkainen[11,12], and Elina Ikonen[1,2]

[1]Department of Anatomy and Stem Cells and Metabolism Research Program, Faculty of Medicine, University of Helsinki, Helsinki, Finland

[2]Minerva Foundation Institute for Medical Research, Helsinki, Finland

[3]Department of Pathology, University of Helsinki and Helsinki University Hospital, Helsinki, Finland

[4]Department of Oral Pathology and Radiology, University of Turku, Turku, Finland

[5]Clinical Protein Science & Imaging, Department of Biomedical Engineering, Lund University, Lund, Sweden

[6]Division of Oncology, Department of Clinical Sciences, Lund, Lund University, Lund, Sweden

[7]Data Convergence Drug Research Center, Therapeutics and Biotechnology Division, Korea Research Institute of Chemical Technology (KRICT), Daejeon, Republic of Korea

[8]Biomarkers and Epidemiology, Department of Clinical Sciences, Lund, Lund University, Lund, Sweden

[9]Synthetic and Systems Biology Unit, Biological Research Centre, Eotvos Lorand Research Network, Szeged, Hungary

[10]Institute of Biotechnology/HiLIFE, University of Helsinki, Helsinki, Finland

[11]Department of Surgery, University of Helsinki and Helsinki University Hospital, Helsinki, Finland

[12]Translational Cancer Medicine Program, University of Helsinki

[13]Section for Clinical Chemistry, Department of Translational Medicine, Lund University, Skåne University Hospital Malmö, Malmö, Sweden

[14]Institute for Molecular Medicine Finland-FIMM, Helsinki Institute of Life Science-HiLIFE, University of Helsinki, Helsinki, Finland

[15]Single-Cell Technologies Ltd., Szeged, Hungary

[*]These authors contributed equally

Contents

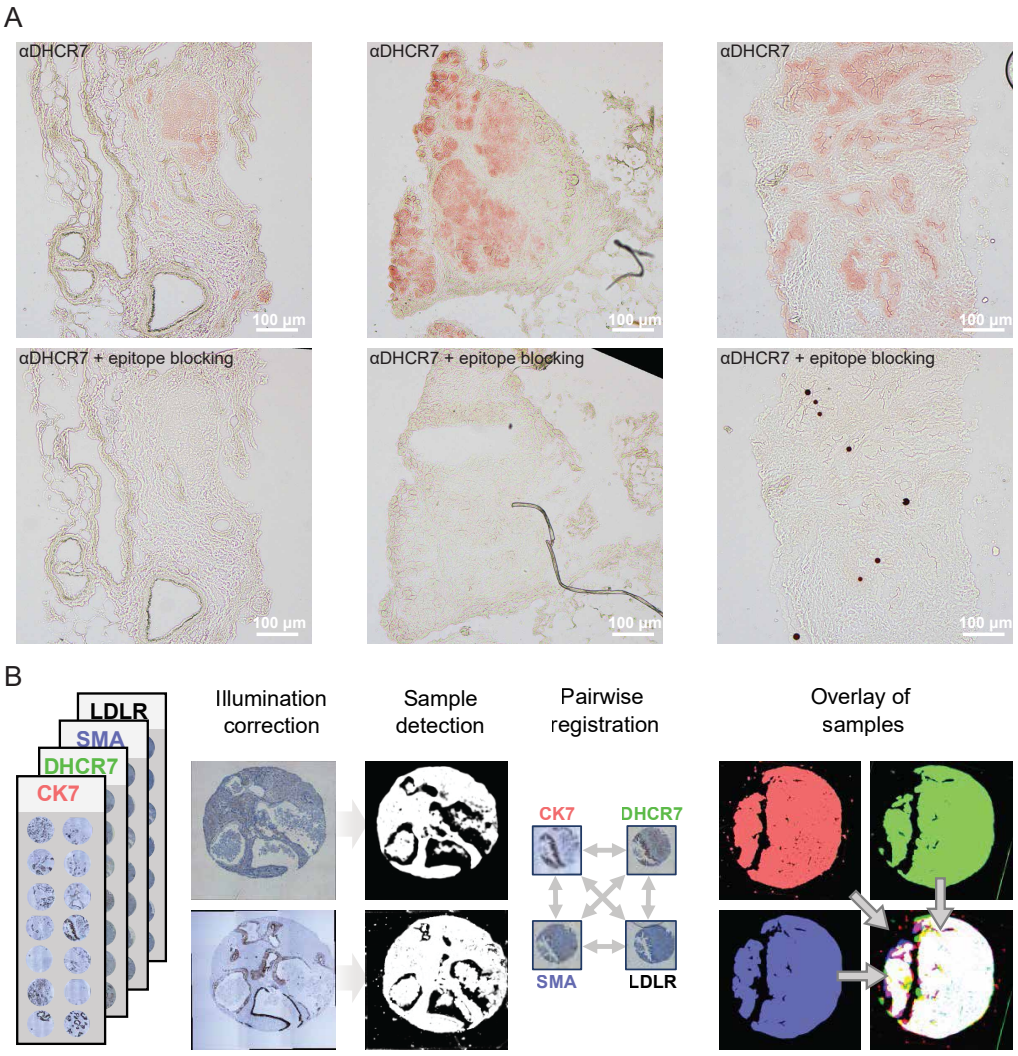

Supplemental Figure 1: Validation of DHCR7 antibody and overview of the TMA processing pipeline A) DHCR7 antibody validation by epitope blocking. Top row: no blocking, bottom row: blocking of epitope using antigenic peptide using sequential sections. B) Overview of TMA processing. Sequential PDAC TMA slides were stained with antibodies against the indicated proteins, illumination corrected, and overlaid using a robust affine image registration framework coupled with supervised machine learning.

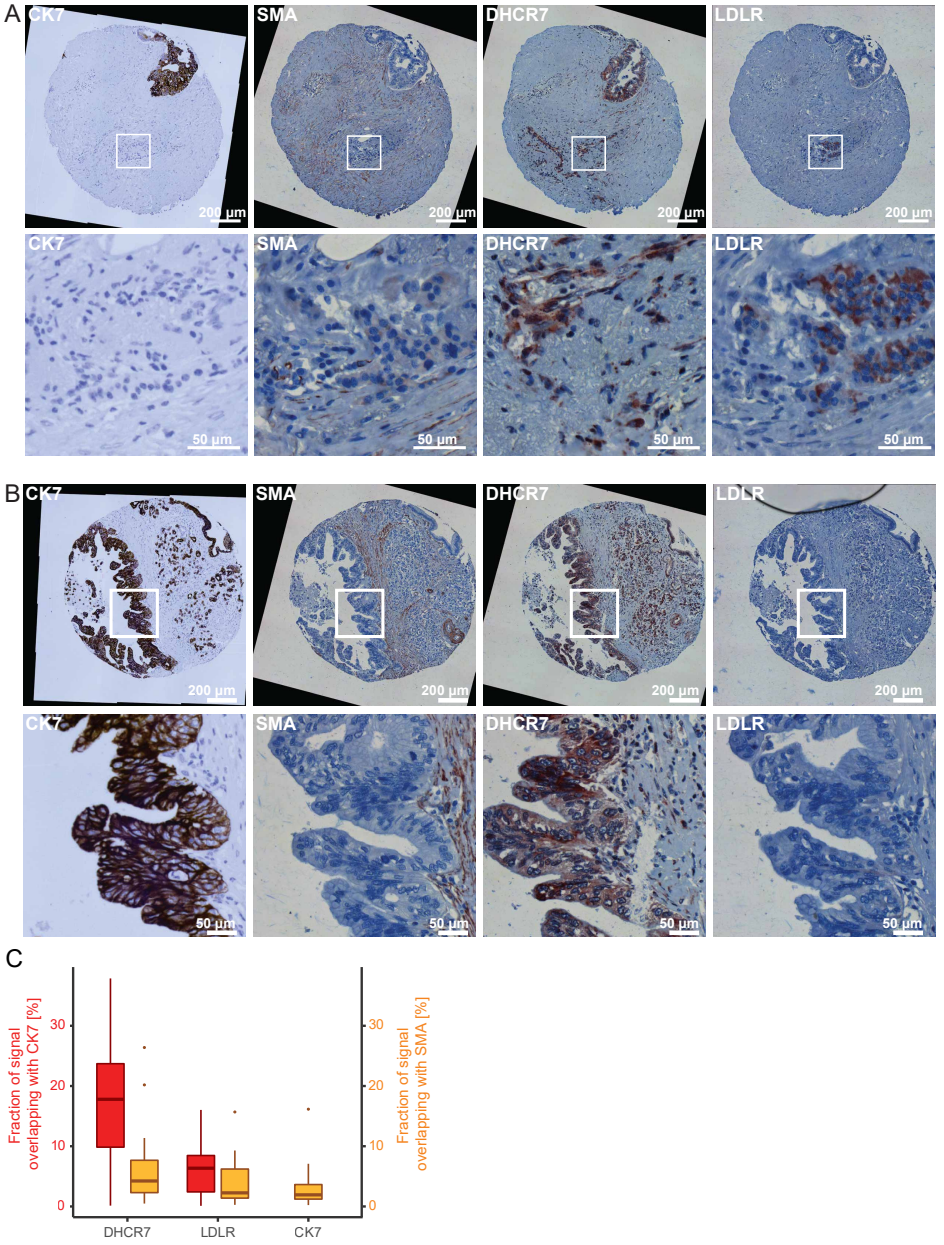

Supplemental Figure 2: Immunohistochemical staining of TMAs shows higher cholesterol biosynthetic enzyme levels in neoplastic parenchyma than in neoplastic stroma. A) Exemplary image of LDLR-positive sample region. LDLR signal arises mainly from a structure resembling a Langerhans islet. White boxes indicate the location of the insets in the bottom row. B) Exemplary TMA spots depicting DHCR7 and LDLR immunostainings between neoplastic parenchymal (CK7 positive) and stromal (SMA positive) compartments. C) Manders colocalization values for signals overlapping with either CK7 or SMA. 42 samples from 24 patients. The hinges indicate the first and third quartiles, error bars (whiskers) show the furthermost observation from the hinges within interquartile range multiplied by 1.5. Ratios of samples with p-value less than 0.05 in Costes' randomization from left to right were 90.5%, 81.0%, 45.2%, 47.6%, 45.2% respectively.

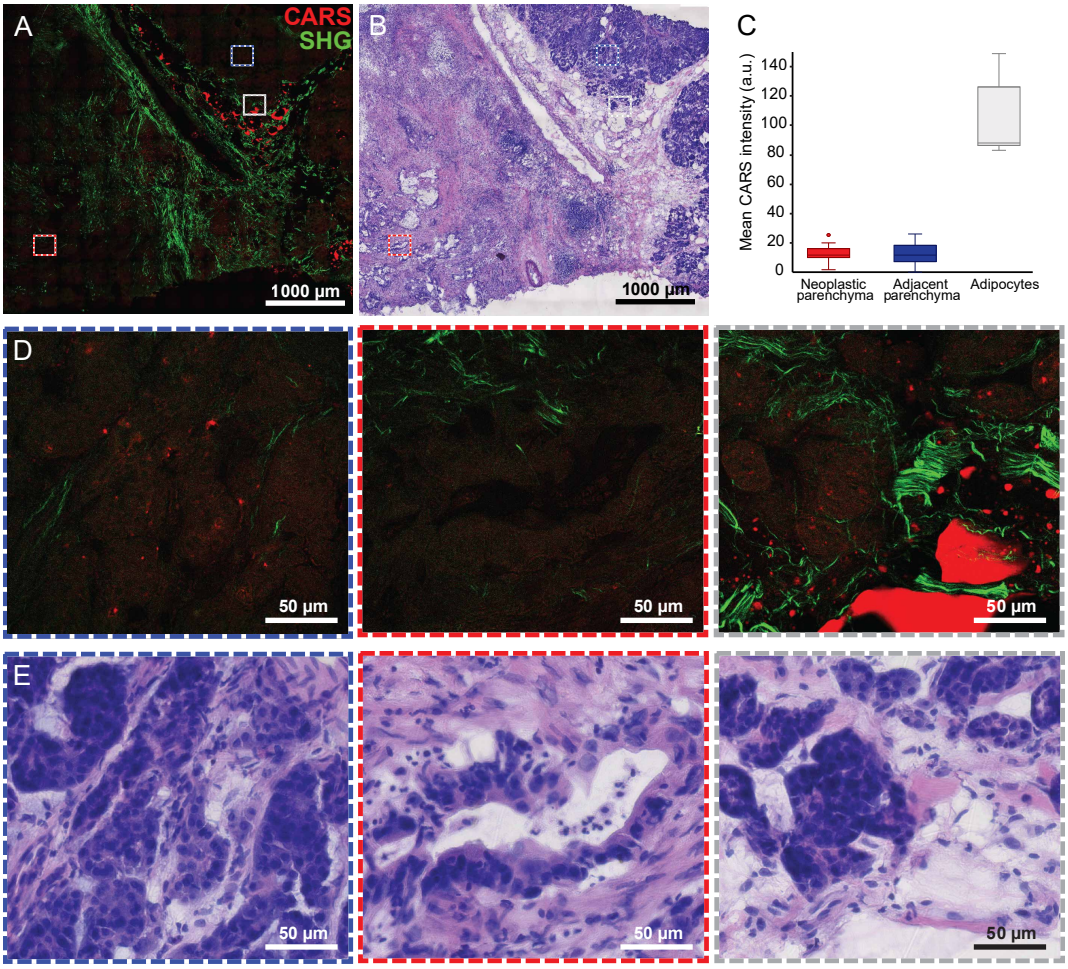

Supplemental Figure 3: Lipid accumulation in human PDAC samples quantified with non-linear imaging. A) Overview of an exemplary PDAC cryosection imaged by CARS (red) and SHG (green) and B) HE-staining of the same section. C) Quantification of the lipid-specific CARS signal from tissue areas representing neoplastic parenchyma, adjacent parenchyma, and adipocytes (N=18, 6, and 8 areas, respectively). Whiskers show interquartile range. D) Insets from A). Note that even though no major lipid deposition can be found in the tumor and the adjacent acinar area, red signal compatible with small lipid droplets are observable in the adjacent parenchymal region. E) Insets from B). Blue outline: adjacent parenchyma, red outline: neoplastic parenchyma, grey outline: area containing adipocytes.

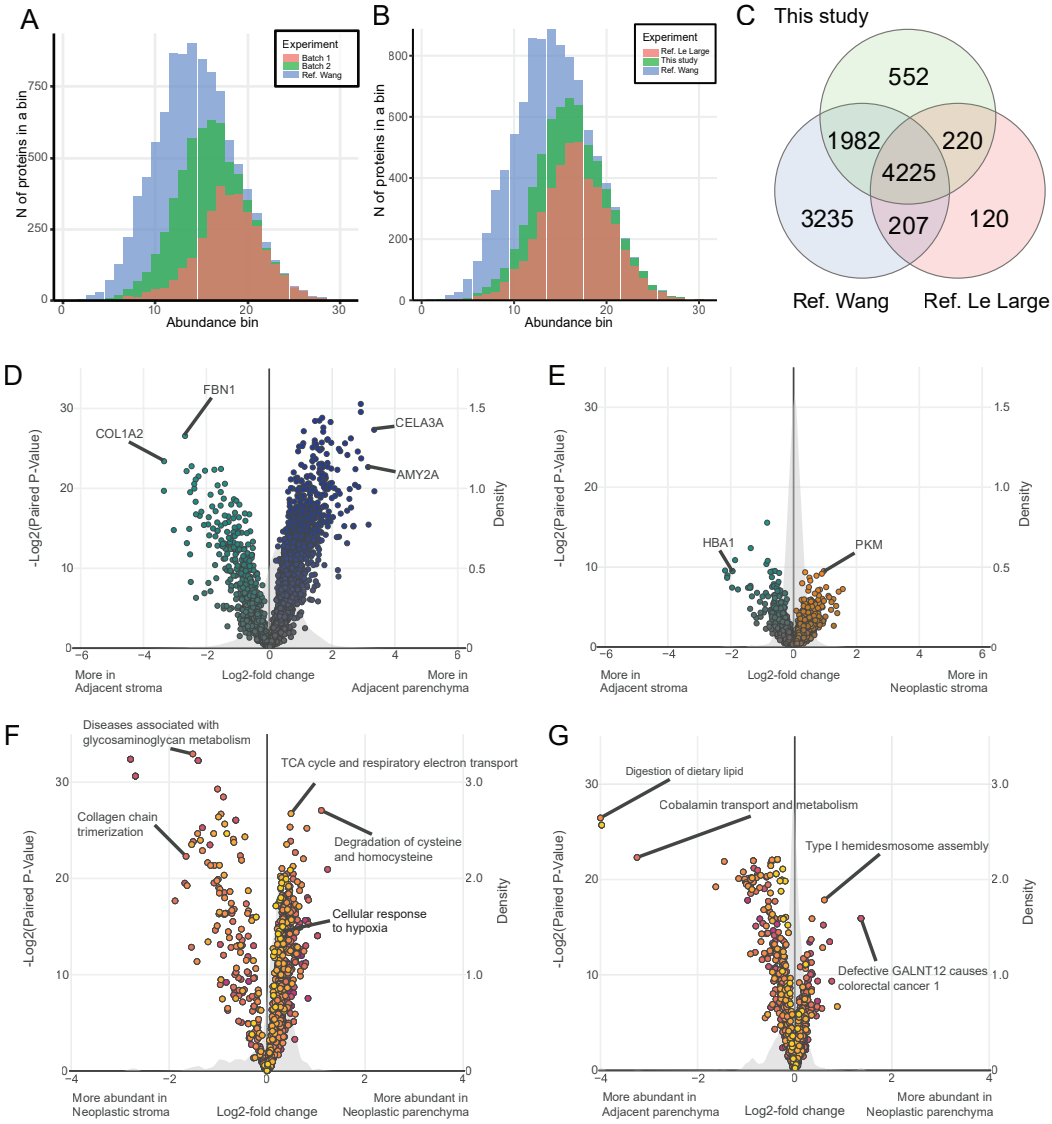

Supplemental Figure 4: Comparison of proteomic coverages and differential protein expressions between tissue types. A) Comparison of batches 1 and 2 of this study with a reference proteome of the entire pancreas [1]. Batch 2 samples are larger and accordingly have more unique proteins than batch 1. B) Comparison of proteomic coverages in abundance bins between three studies (this study and studies by [1, 2]). C) Venn diagram of unique pancreatic proteins based on the three studies as in B. Volcano plots in D-G show paired differential pathway expression or normalized protein abundance on the x-axis and -log2(p.value) from paired, two-sided t.test on the left y-axis. The density of the protein abundances is shown as a grey area on the plot background and on the right y-axis. D) Comparison of adjacent parenchyma and stroma at protein level. E) Comparison of the stromas at protein level. F) Comparison of neoplastic parenchyma and stroma at pathway level. G) Comparison of the neoplastic and adjacent parenchyma at pathway level.

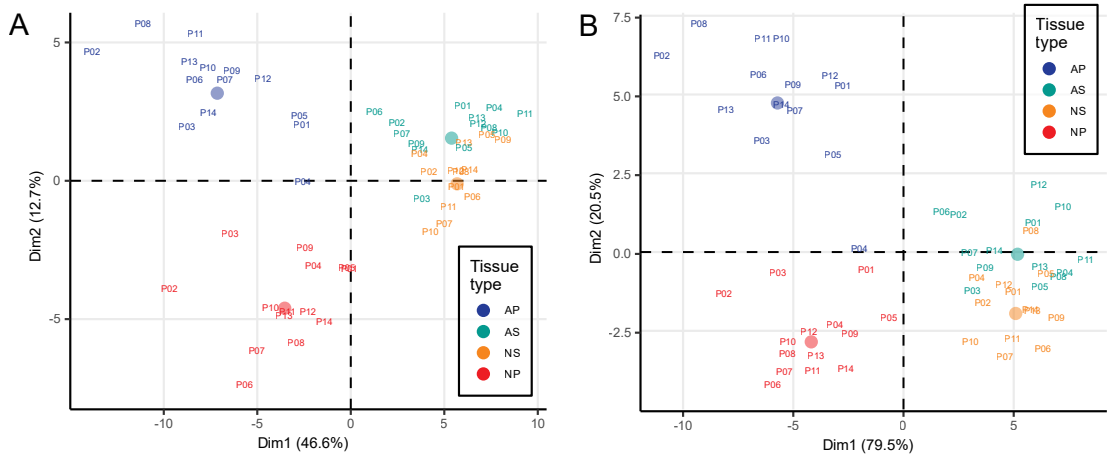

Supplemental Figure 5: Pathway level PCA plots. In this figure, data is filtered to Reactome level 2-3 nodes. A) Normal PCA B) Sparse PCA of the same data, with 55 of 1095 of the pathways present and resolving top 3 dimensions.

ID	Dim	Coord	Contrib	Tot.Contr.	Cum.Contr.	Name	AP	AS	NP	NS
R-HSA-71064	1	-4.33	13.2%	11.7%	11.7%	Lysine catabolism	1.35	0.31	1.17	0.41
R-HSA-8948216	1	3.38	8.0%	7.1%	18.8%	Collagen chain trimerization	1.07	2.25	0.51	2.13
R-HSA-2243919	1	3.29	7.6%	6.8%	25.6%	Crosslinking of collagen fibrils	1.50	2.55	0.69	2.53
R-HSA-1614558	1	-3.25	7.4%	6.6%	32.2%	Degradation of cysteine and homocysteine	-0.15	-0.91	0.19	-0.93
R-HSA-71403	1	-3.19	7.2%	6.4%	38.6%	Citric acid cycle (TCA cycle)	1.04	0.08	0.79	0.09
R-HSA-3000480	1	3.18	7.1%	6.3%	44.9%	Scavenging by Class A Receptors	2.22	3.19	1.54	3.14
R-HSA-8876493	1	-3.05	6.5%	5.8%	50.7%	InlA-mediated entry of Listeria monocytogenes into host cells	1.56	0.72	1.69	0.84
R-HSA-5693571	1	-2.49	4.4%	3.9%	54.6%	Nonhomologous End-Joining (NHEJ)	1.04	0.51	0.98	0.67
R-HSA-8937144	1	-2.26	3.6%	3.2%	57.8%	Aryl hydrocarbon receptor signalling	0.83	0.47	1.29	0.51
R-HSA-140875	1	2.23	3.5%	3.1%	60.9%	Common Pathway of Fibrin Clot Formation	-0.02	1.06	0.00	1.01
R-HSA-2151201	1	-2.14	3.2%	2.9%	63.7%	Transcriptional activation of mitochondrial biogenesis	1.18	0.42	0.97	0.36
R-HSA-8949664	1	-1.98	2.8%	2.5%	66.2%	Processing of SMDT1	0.31	-0.28	0.51	-0.18
R-HSA-430116	1	1.78	2.2%	2.0%	68.2%	GP1b-IX-V activation signalling	2.77	4.20	2.84	4.24
R-HSA-83936	1	-1.77	2.2%	2.0%	70.1%	Transport of nucleosides and free purine and pyrimidine bases across the plasma membrane	0.12	-0.68	-0.05	-0.64
R-HSA-8876725	1	-1.67	2.0%	1.7%	71.9%	Protein methylation	3.81	2.68	3.11	2.75
R-HSA-9633012	1	-1.62	1.8%	1.6%	73.5%	Response of EIF2AK4 (GCN2) to amino acid deficiency	1.72	0.33	0.72	0.22
R-HSA-156902	1	-1.62	1.8%	1.6%	75.2%	Peptide chain elongation	1.86	0.45	0.83	0.35
R-HSA-77289	1	-1.41	1.4%	1.2%	76.4%	Mitochondrial Fatty Acid Beta-Oxidation	0.51	-0.34	0.11	-0.39
R-HSA-2408557	1	-1.36	1.3%	1.2%	77.6%	Selenocysteine synthesis	1.70	0.32	0.69	0.20
R-HSA-156842	1	-1.32	1.2%	1.1%	78.7%	Eukaryotic Translation Elongation	1.88	0.48	0.85	0.38
R-HSA-72764	1	-1.30	1.2%	1.1%	79.7%	Eukaryotic Translation Termination	1.72	0.34	0.72	0.24
R-HSA-6791226	1	-1.23	1.1%	1.0%	80.7%	Major pathway of rRNA processing in the nucleolus and cytosol	1.60	0.28	0.65	0.18
R-HSA-196071	1	-1.22	1.0%	0.9%	81.6%	Metabolism of steroid hormones	-0.32	-0.70	-0.03	-0.87
R-HSA-156827	1	-1.15	0.9%	0.8%	82.4%	L13a-mediated translational silencing of Ceruloplasmin expression	1.54	0.25	0.66	0.18
R-HSA-8868773	1	-1.15	0.9%	0.8%	83.3%	rRNA processing in the nucleus and cytosol	1.49	0.20	0.58	0.11
R-HSA-1834941	1	-1.07	0.8%	0.7%	84.0%	STING mediated induction of host immune responses	0.67	0.23	0.82	0.35
R-HSA-975956	1	-0.99	0.7%	0.6%	84.6%	Nonsense Mediated Decay (NMD) independent of the Exon Junction Complex (EJC)	1.64	0.30	0.68	0.20
R-HSA-2408522	1	-0.97	0.7%	0.6%	85.2%	Selenoamino acid metabolism	1.46	0.20	0.57	0.11
R-HSA-72737	1	-0.88	0.5%	0.5%	85.7%	Cap-dependent Translation Initiation	1.42	0.17	0.57	0.10
R-HSA-72613	1	-0.88	0.5%	0.5%	86.1%	Eukaryotic Translation Initiation	1.42	0.17	0.57	0.10
R-HSA-1799339	1	-0.80	0.5%	0.4%	86.5%	SRP-dependent cotranslational protein targeting to membrane	1.58	0.19	0.52	0.07
R-HSA-8963901	1	0.79	0.4%	0.4%	86.9%	Chylomicron remodeling	0.03	0.91	-0.01	0.94
R-HSA-3000471	1	0.76	0.4%	0.4%	87.3%	Scavenging by Class B Receptors	0.69	1.62	0.37	1.47
R-HSA-975957	1	-0.67	0.3%	0.3%	87.6%	Nonsense Mediated Decay (NMD) enhanced by the Exon Junction Complex (EJC)	1.51	0.24	0.62	0.15
R-HSA-5661270	1	-0.66	0.3%	0.3%	87.8%	Formation of xylulose-5-phosphate	0.73	-0.04	0.43	-0.17
R-HSA-9033500	1	-0.60	0.3%	0.2%	88.1%	TYSND1 cleaves peroxisomal proteins	-0.39	-0.87	-0.07	-0.81
R-HSA-111367	1	-0.50	0.2%	0.2%	88.2%	SLBP independent Processing of Histone Pre-mRNAs	-0.90	-1.34	-0.77	-1.31
R-HSA-77588	1	-0.50	0.2%	0.2%	88.4%	SLBP Dependent Processing of Replication-Dependent Histone Pre-mRNAs	-0.90	-1.34	-0.77	-1.31
R-HSA-194068	1	-0.38	0.1%	0.1%	88.5%	Bile acid and bile salt metabolism	-0.24	-0.68	-0.09	-0.70
R-HSA-5675482	1	-0.32	0.1%	0.1%	88.5%	Regulation of necroptotic cell death	1.38	0.95	1.60	0.94
R-HSA-5213460	1	-0.32	0.1%	0.1%	88.6%	RIPK1-mediated regulated necrosis	1.38	0.95	1.60	0.94
R-HSA-1614635	1	-0.27	0.1%	0.0%	88.6%	Sulfur amino acid metabolism	-0.12	-0.81	-0.04	-0.86
R-HSA-499943	1	-0.26	0.0%	0.0%	88.7%	Interconversion of nucleotide di- and triphosphates	-0.05	-0.45	0.30	-0.40
R-HSA-168273	1	-0.25	0.0%	0.0%	88.7%	Influenza Viral RNA Transcription and Replication	1.42	0.20	0.54	0.11
R-HSA-71406	1	-0.23	0.0%	0.0%	88.8%	Pyruvate metabolism and Citric Acid (TCA) cycle	0.55	-0.17	0.41	-0.14
R-HSA-2129379	1	0.18	0.0%	0.0%	88.8%	Molecules associated with elastic fibres	-0.01	1.20	0.03	1.41
R-HSA-1638074	1	0.15	0.0%	0.0%	88.8%	Keratan sulfate/keratin metabolism	0.37	1.38	0.06	1.54
R-HSA-2408550	1	-0.11	0.0%	0.0%	88.8%	Metabolism of ingested H2SeO4 and H2SeO3 into H2Se	0.06	-0.41	0.19	-0.43
R-HSA-5686938	1	0.10	0.0%	0.0%	88.8%	Regulation of TLR by endogenous ligand	0.64	1.56	0.66	1.63
R-HSA-70370	1	-0.05	0.0%	0.0%	88.8%	Galactose catabolism	0.52	-0.08	0.59	-0.15
R-HSA-192456	2	3.29	60.6%	6.8%	95.6%	Digestion of dietary lipid	3.69	0.90	-0.31	-0.13
R-HSA-196741	2	2.43	33.0%	3.7%	99.3%	Cobalamin (Cbl, vitamin B12) transport and metabolism	2.44	0.20	-0.80	-0.53
R-HSA-3000471	2	0.90	4.5%	0.5%	99.8%	Scavenging by Class B Receptors	0.69	1.62	0.37	1.47
R-HSA-1592389	2	0.38	0.8%	0.1%	99.9%	Activation of Matrix Metalloproteinases	0.84	0.43	-0.61	-0.03
R-HSA-977347	2	0.38	0.8%	0.1%	100.0%	Serine biosynthesis	0.87	-0.36	-0.75	-0.49
R-HSA-8866423	2	0.21	0.3%	0.0%	100.0%	VLDL assembly	1.71	2.06	1.04	1.67

Supplemental Table 1: Pathways most contributing for sparse PCA dimensions. Pathway loadings and contributions to the explained variance for the pathway-level sparse PCA displayed in Fig. S5B.

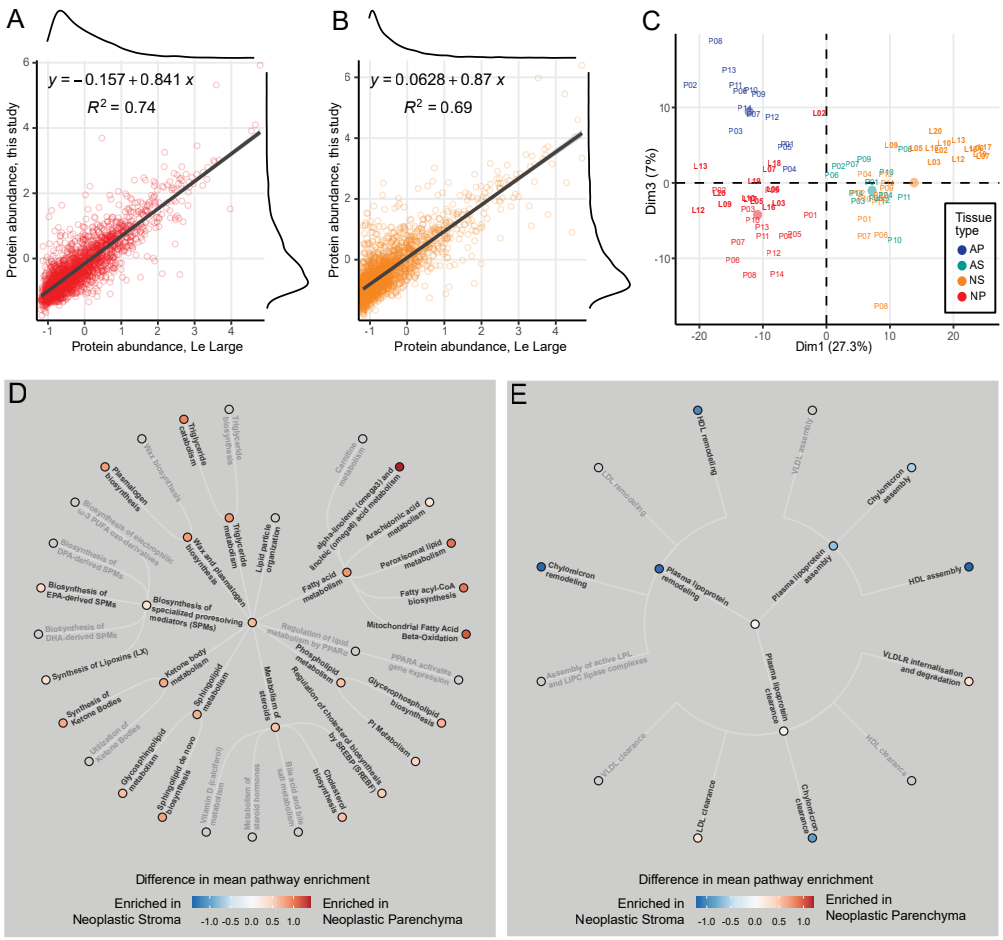

Supplemental Figure 6: Distribution of metabolic pathway enrichments between neoplastic parenchyma and stroma in the study by Le Large et al. A) Correlation of protein abundances between Le Large, et al. [2] and this study for neoplastic parenchymal samples. B) Correlation of protein abundances between Le Large et al., and this study for neoplastic stromal samples. C) PCA dimensions 1 and 3 using normalized data from this study and Le Large et al. Samples displayed with bold text and starting with the letter L arise from Le Large et al., samples from this study have a plain text starting with the letter P. D-E) Enrichment differences in Le Large et al. between neoplastic parenchyma and stroma for Reactome pathways, similar to Figure 3. The center node represents a Reactome pathway (D: Lipid metabolism; E: Plasma lipoprotein assembly, remodeling and clearance) and nodes connected to it represent the two underlying hierarchical levels.

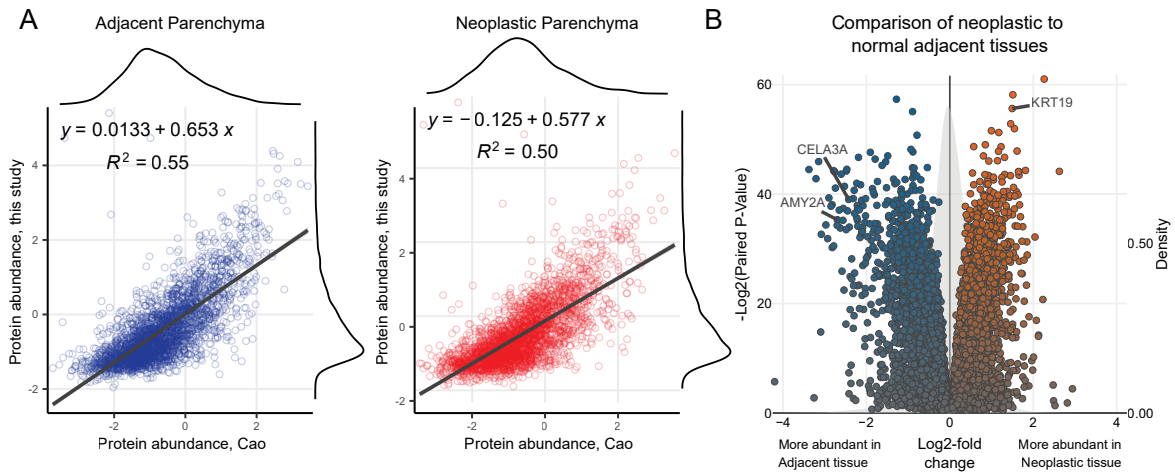

Supplemental Figure 7: Protein abundances and differential expressions are similar in the Cao et al. and this study. A) Correlation of housekeeping normalized protein abundances between Cao et al. [3] and this study for adjacent and neoplastic samples. B) Differential protein expression between the adjacent and neoplastic tissues in the Cao et al. study.

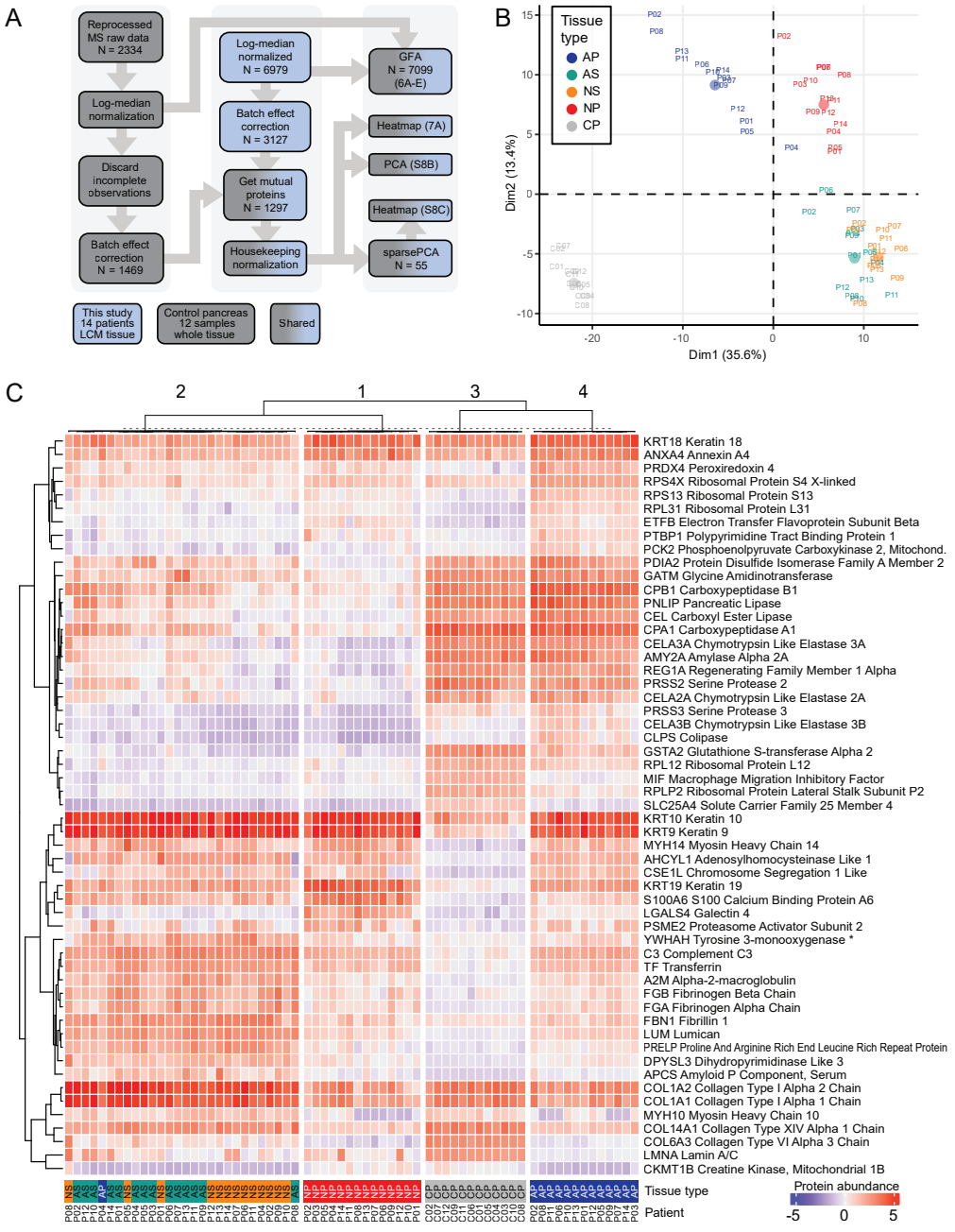

Supplemental Figure 8: Adjacent parenchyma differs from the control pancreas. A) Data processing flow for the inclusion of control pancreatic proteomes in the analyses. The numbers and letters in the parentheses indicate the figure and the panel where the plot is shown. B) PCA plot of protein abundance values, including the control pancreatic proteomes. C) Heatmap of sparse PCA pruned protein abundances. Samples are clustered with k-means = 4, as suggested by the PCA-plot, while pathways are organized with hierarchical clustering. Tissue type and patient identification as in Fig. 1, and additionally CP, control pancreas.

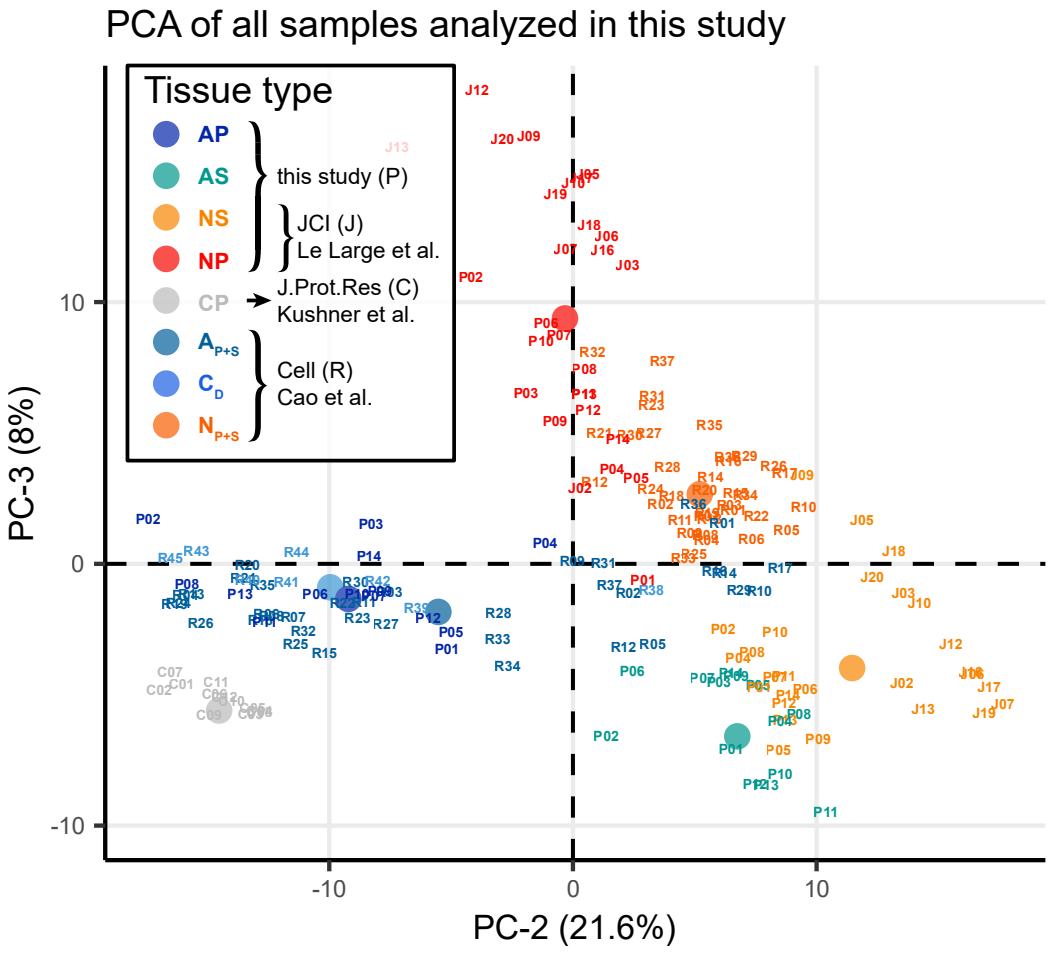

Supplemental Figure 9: Principal component analysis (PCA) of all studies analyzed in this manuscript. PCA plot (PC2-PC3) of the housekeeping normalized protein abundances for all datasets included in this manuscript. the 1st PC was representing variance between the Cao et al. samples and the other 3 studies. Corresponding tissue types cluster together and the non-microdissected tissues are positioned between the corresponding microdissected areas. The healthy control pancreata separate from the tumor-adjacent regions. The similarity between the control ductal and tumor adjacent exocrine samples might be attributed to partial ductal de-differentiation of the acinar cells in the tumor adjacent tissue or the difficulty of separating these cells even with microdissection techniques, due to the anatomical proximity of these cell types. Samples from this study: P#; samples from Le Large et al.: J# [2]; samples from Kushner et al.: C# [4]; samples from Cao et al. resource paper: R# [3]. Tissue type abbreviations AP: Adjacent Parenchyma, AS: Adjacent Stroma, NS: Neoplastic Stroma, NP: Neoplastic Parenchyma, CP: Control Pancreas, A_{P+S}: Adjacent parenchyma and stroma, C_D: Control Ducts, N_{P+S}: Neoplastic parenchyma and stroma.

References

[1] Dongxue Wang, Basak Eraslan, Thomas Wieland, Björn Hallström, Thomas Hopf, Daniel Paul Zolg, Jana Zecha, Anna Asplund, Li-hua Li, Chen Meng, et al. A deep proteome and transcriptome abundance atlas of 29 healthy human tissues. *Molecular systems biology*, 15(2):e8503, 2019.

[2] Tessa YS Le Large, Giulia Mantini, Laura L Meijer, Thang V Pham, Niccola Funel, Nicole CT van Grieken, Bart Kok, Jaco Knol, Hanneke WM van Laarhoven, Sander R Piersma, et al. Microdissected pancreatic cancer proteomes reveal tumor heterogeneity and therapeutic targets. *JCI insight*, 5(15), 2020.

[3] Liwei Cao, Chen Huang, Daniel Cui Zhou, Yingwei Hu, T Mamie Lih, Sara R Savage, Karsten Krug, David J Clark, Michael Schnaubelt, Lijun Chen, et al. Proteogenomic characterization of pancreatic ductal adenocarcinoma. *Cell*, 184(19):5031–5052, 2021.

[4] Irena K Kushner, Geremy Clair, Samuel Owen Purvine, Joon-Yong Lee, Joshua N Adkins, and Samuel H Payne. Individual variability of protein expression in human tissues. *Journal of proteome research*, 17(11):3914–3922, 2018.